Fifth International Conference on CFD in the Process Industries
CSIRO, Melbourne, Australia
13-15 December 2006

USE OF CFD TO PREDICT AND REDUCE EROSION IN AN INDUSTRIAL SLURRY PIPING SYSTEM

Gary BROWN

Alcoa World Alumina Australia, Kwinana Refinery, Kwinana, Western Australia 6167

ABSTRACT

Computational fluid dynamics (CFD) modelling has been applied to determine the cause of erosive failures in slurry piping on the discharge of digester vessels at Alcoa's Wagerup alumina refinery.

In the piping system, the swirling flow exiting the bottom of a digester vessel is turned through ninety degrees using a customised bend. The commercial package CFX-5.7 is used to predict the motion of caustic liquor and bauxite particles through this system using an Eulerian-Lagrangian approach, and an erosion map is developed using the Finnie erosion model. Results from the model predict an accumulation of particles on the wall of the bend at the centre of a slow-moving vortex, and an associated high wear zone, the location of which is in excellent agreement with the observed wear on the plant. As a result of the confidence gained in the CFD model through this work, the model is subsequently used to assess proposed modifications to the bend and a design change based on the model outcomes was successfully implemented on the plant.

NOMENCLATURE

C_D	drag coefficient
d_p	particle diameter
E	erosion rate
$\boldsymbol{g}$	gravitational acceleration
k	fluid turbulent kinetic energy
k_1	erosion model constant
L_s	characteristic length
m	particle mass
n	erosion model constant
p	fluid pressure
r_f	fluid phase volume fraction
r_p	particulate phase volume fraction
S_t	Stokes number
$\boldsymbol{u}_f$	fluid velocity
$\boldsymbol{u}_p$	particle velocity
$\mathbf{v}_R$	particle relative velocity
V_1	particle impact velocity
V_s	characteristic velocity
β	particle mass loading
ε	fluid turbulence dissipation rate
γ_1	particle impact angle
μ_{eff}	effective viscosity for fluid phase
μ_f	fluid dynamic viscosity
ρ_f	fluid density
ρ_p	particle density

INTRODUCTION

At Alcoa's Wagerup alumina refinery in Western Australia the swirling flow exiting digester vessels is turned through ninety degrees in an area referred to as the discharge "pot" before being directed to the next vessel in series (Figure 1). The slurry being transported in this section of the plant consists of bauxite particles in a hot caustic soda solution. The bauxite particles have a high silica content and are hence highly abrasive.

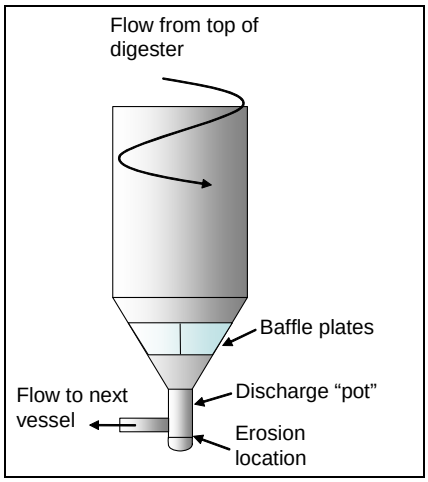

Figure 1: Schematic of lower digester and discharge area

In August 2003 the discharge "pot" in two separate digester vessels failed within twelve hours of each other due to highly localised erosion at an unexpected, but identical, location on each. The erosion was located directly opposite the outlet pipe at a height close to the join between the elliptical head and the straight side wall, as shown in Figures 1 and 2. The failures required the vessels to be immediately taken out of circuit, resulting in a production loss exceeding A$1 million.

An investigation of the failures using a cross-section of staff from engineering and operations groups was immediately conducted using a root cause analysis methodology. This investigation concluded that the most likely cause of the failures was an apparently minor design change made to the bends on all digester vessels during a piping upgrade project completed less than twelve months earlier, and hence that the bends on the remaining digester vessels may also have been at risk of imminent failure.

As a result, an ongoing program of ultrasonic testing was immediately put in place to ensure the integrity of the remaining bends and a computational fluid dynamics (CFD) study was initiated to determine the cause of the

erosion, confirm if there was a systemic problem with the bend design and, if necessary, to assist in the design of modifications to the bends.

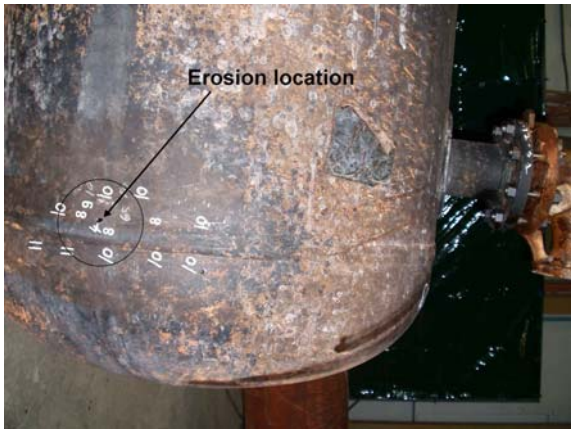

Figure 2: Hole in discharge "pot". Chalk figures indicate metal thickness in mm (initial metal thickness was 12 mm)

This paper describes the use of the commercial package CFX-5.7 to predict the motion of caustic liquor and bauxite particles through a model of the bend system using an Eulerian-Lagrangian approach in conjunction with the k-ε turbulence model, and the development of an erosion map using the Finnie erosion model.

PARTICLE TRANSPORT MODEL SELECTION

The three most common particle transport models, and those most prevalent in commercial CFD codes, are the Eulerian-Eulerian, Eulerian-Lagrangian and drift-flux (or algebraic slip) models. All three of these models could potentially be applied to the simulation of a mineral processing slurry, depending on the exact slurry characteristics and the flow geometry in question. The advantages and disadvantages of each approach have been previously described in detail (Brown, 2002) and are not further discussed here. However, selection of the correct particle transport model for a particular application can be assisted by first calculating the particle mass loading, β, and the Stokes number, S_t.

The particle mass loading is expressed as:

$$\beta = \frac{\text{particulate mass per unit volume of flow}}{\text{fluid mass per unit volume of flow}} = \frac{r_p \rho_p}{r_f \rho_f} \quad (1)$$

where r is a volume fraction, ρ is a density and the subscripts p and f refer to the particle and fluid phases respectively. Significant two-way particle-fluid coupling is generally expected for particle mass loadings greater than 0.2.

The degree to which the particle motion is tied to the fluid motion can be determined through evaluation of the Stokes number. This is defined as the ratio of the particle response time due to viscous drag to a characteristic turbulent eddy time in the carrier fluid. This can be expressed as:

$$S_t = \frac{\rho_p d_p^2 V_s}{18 \mu_f L_s} \quad (2)$$

where d_p is the particle diameter, μ_f is the dynamic viscosity of the carrier fluid and V_s and L_s are characteristic velocity and length scales in the flow.

For large values, S_t>2.0, the particulate flow is highly inertial and, in a confined geometry, would be dominated by particle-wall interactions, whereas for values less than 0.25 the effect of particle-wall interactions on the particle flow is essentially negligible because the particles are more tightly coupled to the fluid through viscous drag (Tu and Fletcher, 1996). At Stokes numbers below 0.05 the particles and carrier fluid are strongly coupled and the particles would be expected to approximately follow the fluid flow.

Model selection

For the digester piping system to be evaluated in the current study the particle mass loading in the bulk flow was calculated to be approximately 0.12 which indicated that it should be possible to neglect two-way particle-fluid coupling.

The Stokes number based on the velocity and pipe diameter in the bend and mean particle size was calculated to be approximately 0.2, which indicated that particle-wall interactions would have a negligible effect on the particle flow and hence that no special treatment of the particle boundary conditions was required.

In consideration of this analysis, the need to consider a wide particle size distribution, and the fact that the built-in erosion models in CFX were integrated with the Lagrangian particle tracking routines, a one-way coupled Eulerian-Lagrangian model was selected for the current study.

EROSION MODELLING

Following the concepts established by Finnie and Bitter, erosion of a solid surface due to particle impacts can be considered to be due to two separate mechanisms, namely deformation wear and cutting wear (Finnie, 1960 and Bitter, 1963).

Deformation wear occurs when repeated particle impacts at high impact angles plastically deform the surface layers of the material, eventually causing material loss through surface fragmentation. Cutting wear occurs due to particle impacts at small angles, with a scratch or cut being formed on the surface if the shear strength of the material is exceeded.

The total erosion rate at a particular point on a surface is found by summing the contributions due to the deformation and cutting mechanisms and depends on the properties of the material, with deformation wear being more significant for hard, brittle materials and cutting wear being more significant for softer, ductile materials. For standard commercial grade steels, as used in most of the bend surfaces in this study, peak erosion rates have been measured to occur at impact angles of 25-30°, indicating that cutting wear dominates (Bitter, 1963).

The other critical factor affecting wear is the particle impact velocity, with both cutting and deformation wear

being proportional to impact velocity raised to a power *n* determined through physical tests. In general *n* is found to vary between 2.0 and 3.0 depending on both the surface and particle materials.

Literature on the used of erosion models in conjunction with CFD predictions in slurry systems of complex geometry is limited. Some authors, for example, have used CFD models to assist with erosion studies through visualisation of the flow patterns through a device, but have not coupled the CFD solution to an erosion model.

Nešić used a CFD model to examine erosion in heat exchangers used in alumina refineries and demonstrated a relationship between the predicted near-wall turbulence intensity and observed erosion rates, but did not make any predictions with an erosion model (Nešić, 2006). Parslow also used a CFD model to visualise the flow patterns and particle trajectories in tee-junctions and bends associated with typical sub-sea oil and gas production facilities. The predictions were compared to erosion patterns obtained through use of a paint-layer technique, but an erosion model was not implemented (Parslow et al., 1999).

In those studies where erosion models have been implemented the approaches have been varied. Wood, for example, used an algebraic slip multi-phase model connected to a component erosion model based on the work of Bitter (Bitter, 1963) and Hashish (Hashish, 1988) to examine erosion due to slurry flow in straight pipes and bends (Wood et al., 2004). In contrast, Wallace used an Eulerian-Lagrangian model to predict erosion due to the slurry flow in choke valves by employing erosion models developed from data-fitting to the results of jet-type wear tests (Wallace et al., 2004). Habib used an Eulerian-Lagrangian multi-phase model and the erosion model of Neilson and Gilchrist (Neilson and Gilchrist, 1968) to examine erosion in sudden pipe contractions (Habib et al., 2004).

It should also be noted that in all of these studies the flow upstream of the device in question was assumed to be fully developed and studies dealing with non-uniform or swirling approach flows are very limited. In one published study, Wood used small-scale physical modelling and CFD to demonstrate that inducing swirl upstream of a piping elbow could reduce slurry erosion rates by creating a more uniform distribution of particles across the bend surface (Wood et al., 2001). Interestingly, a previous study by the author showed that the presence of swirl could lead to localised particle accumulation and correspondingly high erosion rates in piping tee-junctions (Brown, 2002) and this is further observed in the current study. These results reinforce the complexity of studying erosion in slurry piping systems.

In the current study the simplified erosion model of Finnie has been used (Finnie, 1960). This model is available in CFX for use in conjunction with the Lagrangian particle model. The model of Tabakoff and Grant is also available in CFX but was not used in the current study (Grant and Tabakoff, 1975).

The CFX implementation of the Finnie model is as follows;

$$E = k_1 V_1^n f(\gamma_1) \tag{3}$$

$$\begin{aligned} f(\gamma_1) &= \tfrac{1}{3}\cos^2\gamma_1 && 18.5° \le \gamma_1 \le 90° \\ &= \sin(2\gamma_1) - 3\sin^2\gamma_1 && \gamma_1 < 18.5° \end{aligned} \tag{4}$$

where E is the non-dimensional erosion rate, γ_1 is the impact angle with respect to the surface tangent and k_1 and n are constants. In the current study the velocity power, n, was set to 2.0 and the constant k_1 was set to 1.0.

In the CFX implementation an overall erosion rate at each point on the surface is then found by multiplying E by the mass flow carried by the Lagrangian particle impacting the surface, and then summing over all particles. This ultimately leads to an erosion rate density variable with units of kg/s/m^2 which can be displayed in the post-processor, but it needs to be remembered that this only provides a qualitative erosion rate and is not a physical material loss.

EULERIAN-LAGRANGIAN MODEL DESCRIPTION

Governing Equations

As discussed previously, a one-way coupled Eulerian-Lagrangian model was selected for this study. In this approach, the single phase equations for conservation of mass and momentum are:

$$\frac{\partial \rho}{\partial t} + \nabla \cdot (\rho \mathbf{u}) = 0 \tag{5}$$

$$\begin{aligned} &\frac{\partial (\rho \mathbf{u})}{\partial t} + \nabla \cdot (\rho \mathbf{u} \otimes \mathbf{u}) - \nabla \cdot \left\{ \mu_{eff} \left[\nabla \mathbf{u} + (\nabla \mathbf{u})^T \right] \right\} \\ &= -\nabla p + \rho \mathbf{g} \end{aligned} \tag{6}$$

In addition, turbulence closure is achieved through solution of the standard k-ε model, with the k and ε equations taking the form:

$$\nabla.(\rho \mathbf{u} \phi) - \nabla.\left(\frac{\mu_{eff}}{\sigma_\phi} \nabla \phi \right) = S_\phi \tag{7}$$

where ϕ represents either k or ε, σ_ϕ is the turbulent diffusivity of ϕ and S_ϕ is a source term.

Because of the low particle mass loading in the flow, two-way fluid-particle coupling is ignored and the particle trajectories are determined as a post-process after the fluid solution has been obtained. In the Lagrangian approach these trajectories are determined using Newtonian equations of motion;

$$\text{Momentum:} \quad m \frac{d\mathbf{u}_p}{dt} = \mathbf{F} \tag{8}$$

where the force term, F, consists in this case of a drag term;

$$\mathbf{F}_D = \frac{1}{8} \pi d_p{}^2 C_D \rho_f |\mathbf{v}_R| \mathbf{v}_R \tag{9}$$

and a buoyancy term;

$$\mathbf{F}_B = \frac{1}{6}\pi d_p{}^3(\rho_p - \rho_f)\mathbf{g} \qquad (10)$$

Turbulent particle dispersion was also activated. Using this technique, a random velocity component is added to the mean fluid velocity to account for fluid turbulence. This random velocity component tends to prevent particles from becoming "stuck" in wall boundary layers and also pushes a larger number of particles into any recirculation zones that may exist within the device being modelled.

Computational Domain and Numerical Procedure

Digesters are tall cylindrical vessels with a single inlet near the top of the vessel. The cylinder then contracts in a cone at the bottom of the vessel to a single central outlet (see Figure 1). The model used in the current study starts part way down the cone at the bottom of the vessel and includes the cross-piece baffle designed to straighten the flow prior to the digester outlet, the discharge "pot" region and a small section of the piping which leads to the next digester vessel.

The digester outlet model was discretised using an unstructured tetrahedral mesh comprising of approximately 700,000 elements. Five layers of prismatic elements were used at the walls to provide better resolution of the wall boundary layer. Mesh controls were used to refine the mesh near the leading and trailing edges of the cross-piece baffle. The surface mesh and computational domain are shown in Figure 3.

The conservation equations for mass, momentum and fluid turbulence were solved within the commercial code CFX-5.7 using a finite volume technique. Convection terms in the momentum equations were discretised using a second-order accurate scheme.

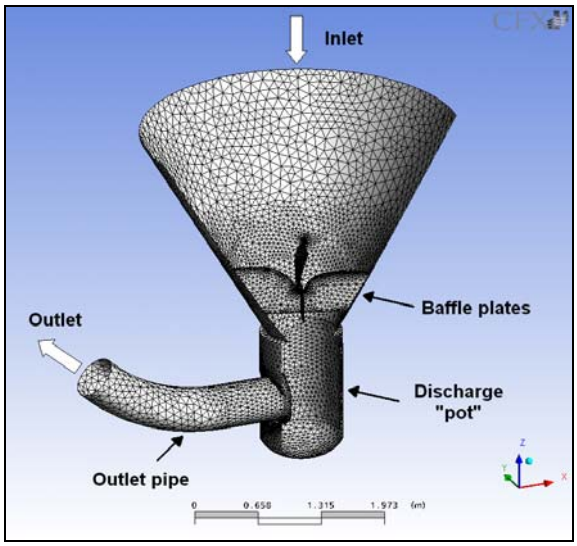

Figure 3: Computational domain and surface mesh.

Boundary Conditions

The correct inlet velocity profile for the model was established by first running a simulation of the entire digester vessel. The velocity profile on a horizontal plane part way down the digester cone was then exported to a spreadsheet using the CFX post-processor. A polynomial for swirl velocity as a function of radius was developed and then used to specify the velocity profile at the inlet to the digester outlet model. In later versions of CFX a more accurate transfer of the velocity profile would be possible using a built-in "profile boundary condition" option which allows variables to be interpolated from a specified plane in one set of results to a specified plane in another simulation.

The particles were assumed to be randomly distributed at the inlet and, due to the low Stokes number, the particle velocity distribution was assumed to be identical to that for the fluid phase. The particle size distribution was specified using a Rosin Rammler distribution based on slurry samples from the plant. A zero gradient condition was applied at the outlet.

Standard no-slip wall functions were applied at all solid surfaces for the fluid phase and the coefficient of restitution for the particles was left at the default value of 1.0. Using a more accurate figure was not considered important because the low Stokes number indicated that wall interactions would not be important in the flow.

SIMULATION RESULTS

The highly localised erosion shown in Figure 2 had not been observed prior to an apparently minor design change made to the outlet design during a piping upgrade project. The pre-upgrade design was therefore simulated first to provide a reference for further simulations and to help validate the model.

It was found that the flow would not converge as a steady state and hence the model was switched to transient solution. The transient was run for 20 s of real time using time steps of 0.1 s, with convergence achieved in 3-5 iterations per time step. In CFX-5.7 it was not possible to use Lagrangian particle tracks in conjunction with a transient flow, and hence to develop an instantaneous erosion map at several points in time the flow field was saved every 4 s and particle tracks were then run on each of these result files as a post-process.

Flow streamlines at one time step are shown in Figure 4 for the initial design. They show a slow, recirculating, flow in the base of the discharge "pot", with high velocities at the entrance to the outlet pipe. Although the flow was transient, this same overall flow structure was evident at all time steps. An erosion map at the same time step is shown in Figure 5. Not surprisingly, the erosion map shows significant erosion around the entrance to the discharge pipe. This agreed well with observations on the plant and the high erosion rates experienced around the entrance to the exit pipe were actually the reason that this part of the design was modified by engineers during the piping upgrade project.

In the modified design, the diameter of the outlet pipe was increased and a liner of hardened material (cast white iron) was also placed inside the entrance to the outlet pipe. This liner was extended out into the discharge "pot" (see Figure 6) such that any erosion occurring at the entrance to the outlet pipe would now be moved away from the main walls, which were only mild steel.

Flow streamlines for the modified design at one of the time steps in the solution are shown in Figure 6. This shows the formation of a vortex in the lower part of the discharge "pot", with the base of the vortex attached to the

wall opposite the outlet pipe, at a vertical position close to the join between the vertical side wall and the elliptical head. Examination of particle trajectories showed that particles entering the base of the discharge "pot" concentrate at the base of the vortex, and hence the erosion map in Figure 7 shows a high relative erosion rate at this point – in this case due to a large number of low angle impacts rather than high impact velocities. The predicted erosion location at the base of the vortex was found to be in close agreement with the actual erosion location on the plant as shown in Figure 2. Examination of the transient results showed that the flow in the bottom of the discharge "pot" was periodic, with this vortex being continuously created and then destroyed over a period of approximately 10 seconds.

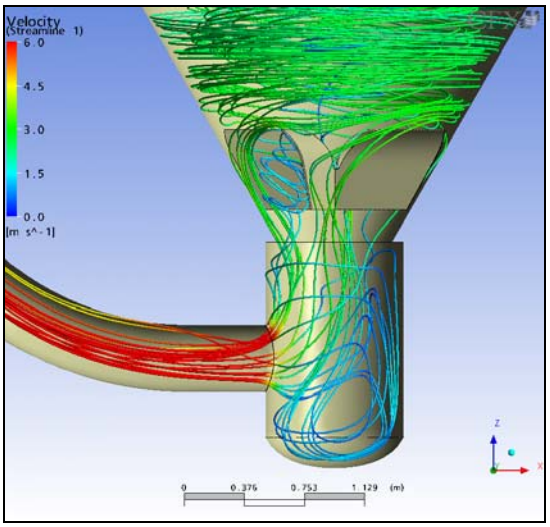

Figure 4: Flow streamlines - initial piping design.

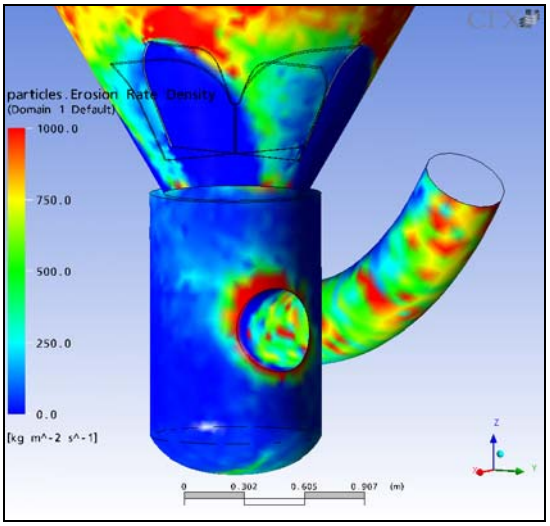

Figure 5: Erosion map – initial piping design.

It is interesting to note that the vortex erosion seen here closely resembles erosion seen by the author in other similar scenarios, such as the erosion caused by the swirling flow through piping tee-junctions at Alcoa's Pinjarra refinery (Brown, 2002).

This result confirmed that the failure of the two discharge "pots" on the plant was due to the apparently minor design change made during the upgrade project. It wasn't completely clear why the extension of the outlet pipe stub into the discharge "pot" altered the flow so significantly, but there is obviously still some vorticity in the flow downstream of the cross-piece baffle which allows the formation of a periodic vortex to be triggered under the right conditions.

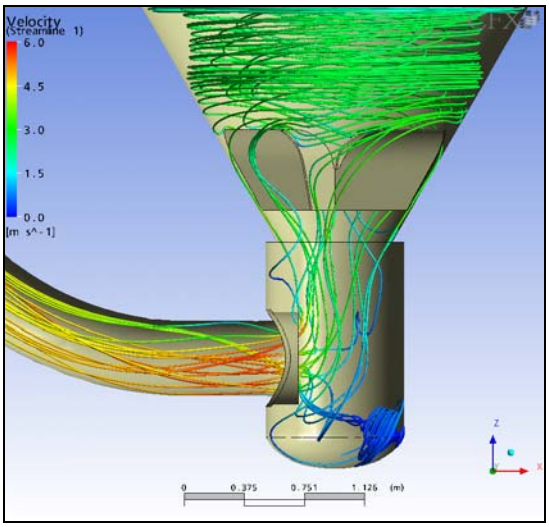

Figure 6: Flow streamlines - modified design after piping upgrade.

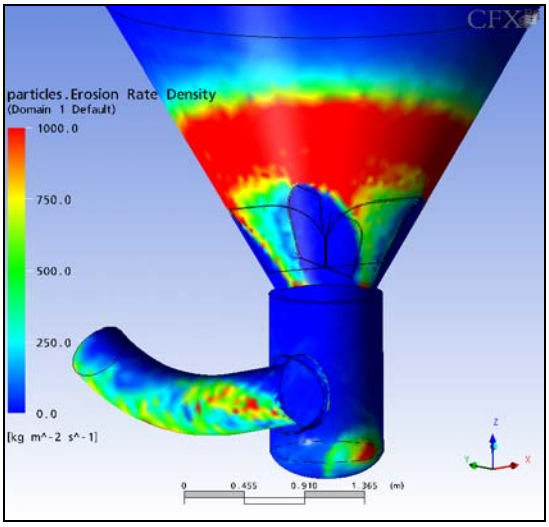

Figure 7: Erosion map - modified design after piping upgrade.

The ability of the CFD analysis to predict the cause of the failure generated significant confidence in the modelling within Alcoa's engineering management. As a result, further modelling was initiated to analyse several proposed modifications to the discharge "pot" which were intended to eliminate both the vortex erosion and the earlier erosion experienced around the entrance to the outlet pipe. A modified design recommended as a result of this modelling was subsequently installed across all digester vessels on the plant and has been operating successfully for several years.

One limitation of the study presented here is that the same erosion model and model constants were used on all of the walls in the model, even though several different materials were used in the real system. The Finnie model used

results in a maximum erosion rate at an impact angle of approximately 20° above the surface tangent and is therefore strictly only correct for ductile materials such as mild steels. The relative erosion rates predicted in areas where hardened materials are used (such as on the walls of the digester cone and the entrance to the outlet pipe in the modified design) should therefore be treated cautiously.

For example, Figure 8 shows that the model predicts high wear rates on the walls of the cone immediately upstream of the cross-piece baffle and around the baffle tips, which agrees well qualitatively with plant observations (Figure 9). However, the erosion rates predicted around the tips of this baffle are actually higher than those predicted at the base of the vortex in Figure 7 (note the difference in the legend range in Figures 7 and 8) whereas in reality the cone of the digester is found to wear at a much slower rate due to the hardened material used in this region.

It is the author's intention to revisit this work in the future using a more generalised erosion model and employing different model constants to account for the varying material characteristics.

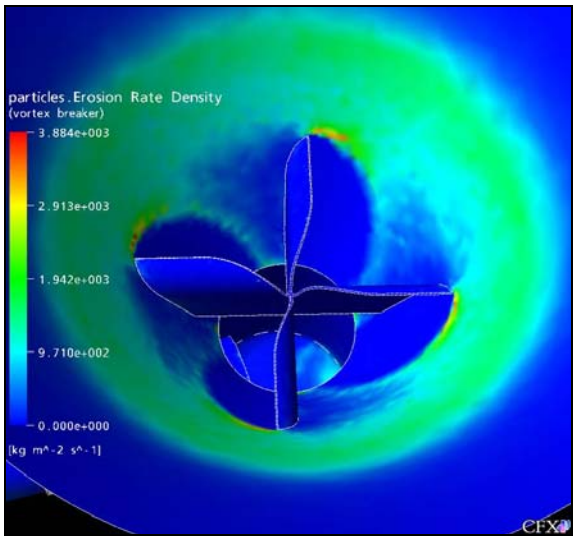

Figure 8: Erosion map for digester cone and cross-piece baffle.

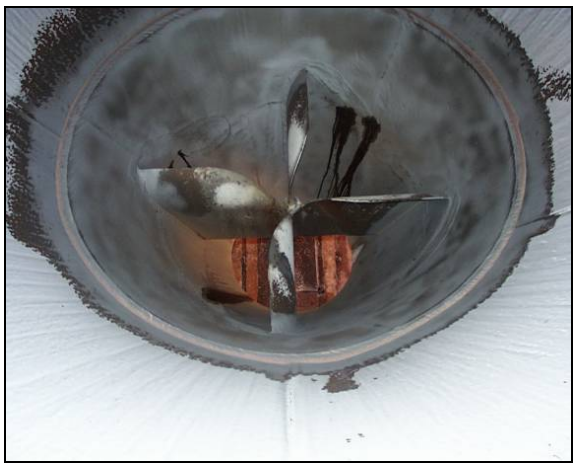

Figure 9: Photograph of digester cone and cross-piece baffle.

CONCLUSIONS

The commercial CFD code CFX-5.7 has been used to investigate the cause of highly localised erosion found to occur in slurry piping on the discharge of digester vessels used on an alumina refinery. The motion of caustic liquor and bauxite particles through this system has been predicted using an Eulerian-Lagrangian approach in conjunction with a k-ε turbulence model, and an erosion map has been developed using the Finnie erosion model

The modelling was able to successfully predict the cause of the erosion and was subsequently used in the development of a new piping design which has been successfully implemented on the plant. This resulted in increased confidence in CFD within Alcoa and a more proactive approach to using CFD as a tool in the engineering design process, rather than only to investigate problems after they've occurred.

REFERENCES

BITTER, J.G.A. (1963), "A study of erosion phenomena: Parts 1 and 2, *Wear*, **6**, 5-21 & 169-190.

BROWN, G.J. (2002), "Erosion prediction in slurry pipeline tee-junctions", *Appl. Math. Modelling*, **26**, 155-170.

FINNIE, I. (1960), "Erosion of surfaces by solid particles", *Wear*, **3**, 87-103.

GRANT, G. and TABAKOFF, W. (1975), "Erosion prediction in turbomachinery resulting from environmental solid particles", J. Aircraft, Vol. 12, No. 5, 471-478.

HABIB, M.A., BADR, H.M., BEN-MANSOUR, R. and SAID, S.A.M. (2004) "Numerical calculations of erosion in an abrupt pipe contraction of different contraction ratios" , *Int. J. Numer. Meth. Fluids*, **46**, 19-35

HASHISH, M. (1988), "An improved model of erosion by solid particles", *Proc. of the Seventh Int. Conf. on Erosion by Liquid and Solid Impact*, paper 66, Cavendish Laboratory.

NEŠIĆ, S. (2006), "Using computational fluid dynamics in combating erosion-corrosion", *Chem. Eng. Sci*., **61**, 4086-4097

NEILSON, J.H. and GILCHRIST, A. (1968), "Erosion by a stream of solid particles", *Wear*, **11**, 111-122.

PARSLOW, G.I, STEPHENSON, D.J., STRUTT, J.E. and TETLOW, S. (1999), "Investigation of solid particle erosion in components of complex geometry", *Wear*, **233-235**, 737-745.

TU, J.Y. and FLETCHER, C.A.J. (1996), "Eulerian modelling of dilute particle-laden gas flows past tubes", *Computational Fluid Dynamics Journal*, **5**, 1-25.

WALLACE, M.S., DEMPSTER, W.M., SCANLON, T., PETERS, J. and McCULLOCH, S. (2004), "Prediction of impact erosion in valve geometries", *Wear*, **256**, 927-936.

WOOD, R.J.K, JONES, T.F., GANESHALINGHAM, J. and MILES, N.J. (2001), "Upstream swirl-induction for reduction of erosion damage from slurries in pipeline bends", *Wear*, **250**, 770-778.

WOOD, R.J.K, JONES, T.F., GANESHALINGHAM, J. and MILES, N.J. (2004), "Comparison of predicted and experimental erosion estimates in slurry ducts", *Wear*, **256**, 937-947.